Tribology International 188 (2023) 108817

Contents lists available at ScienceDirect

Tribology International

journal homepage: www.elsevier.com/locate/triboint

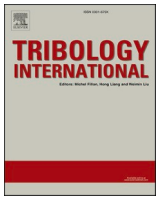

Electrotribodynamics of ball bearings in electrical machines

R. Turnbull [a], R. Rahmani [a,*], S. Paul [b], H. Rahnejat [a,c]

[a] Wolfson School of Mechanical, Electrical and Manufacturing Engineering, Loughborough University, Leicestershire LE11 3TU, UK
[b] Gas Turbine and Transmission Research Centre, Faculty of Engineering, University of Nottingham, Nottingham NG7 2RD, UK
[c] School of Engineering, University of Central Lancashire, Preston PR1 2XQ, UK

ARTICLE INFO

Keywords:
Electro-tribodynamics (ETD)
Tribodynamics of ball bearings
Electric current phenomena in lubricated contacts
Electro discharge damage (EDD)

ABSTRACT

The trend towards electrification presents new challenges in bearing design. One such consideration is the occurrence of electrical discharge contact pathways, which can lead to surface damage. The current study presents a novel comprehensive multiphysics model, incorporating bearing dynamics, mechanics of lubricated rolling element-to-races contacts and electrical contact model for both DC and AC voltages. The model also includes both electrical resistance and capacitance effects in the bearing contacts. Key bearing vibration frequencies such as cage frequency and the bearing base natural frequency along with the voltage supply frequency are observed as influential in the electric current discharge. The developed model enables the prediction of rhythmic fluting patterns commonly observed in the failed bearing applications subject to electrical discharge.

1. Introduction

Rolling element bearings are an integral part of many machines and mechanisms. They are subjected to wear and fatigue [1–3], vibration and noise [4–7] and thermal stability [8,9] issues, which limit their performance. Furthermore, there is a strong trend towards electrification in all forms of transport, particularly light road transport vehicles and some aerospace applications. This trend presents a variety of new challenges in bearing failure [10–13]. An example is the electrically-induced bearing damage caused by the presence of a voltage potential difference between the motor shaft and ground [14]. There are three fundamental causes of voltage differences; (i)- electromagnetic effects due to the emergence of an uneven magnetic flux field, (ii)- build-up of electrostatic charge through accumulation of charged particles, and (iii)- external voltages due to motor excitation [14,15].

Variable frequency drives (VFDs) can cause electric currents to pass through the shaft-bearing system. These currents can cause damages which are manifested by small craters, resembling those created by the Electro-Discharge Machining (EDM) process. There is also frosting, fluting, and pitting of bearing races. They can all cause premature failure of bearings [14–22]. A characteristic damage pattern often takes the form of a periodic ripple-shaped grooves [16–22] around the bearing raceways. Kowal [14] noted the prevalence of fundamental bearing frequencies such as ball-pass frequency in the breakdown patterns, highlighting the influence of electrical insulating ability of the lubricant film thickness. Detecting and diagnosing bearing problems associated with electrical currents can often be challenging as they initially resemble standard bearing failure features. Therefore, understanding the root cause of electrically-induced bearing damage is an important first step in failure diagnosis and monitoring, reducing critical failures and machine downtimes. Therefore, a combined electro-tribo-dynamics model of the ball bearing would be required as a multi-physics tool to account for the variations in the lubricant film thickness, and thus, the electrical conductivity of the bearing.

Dynamics of rolling element bearings comprises complex motions of the complement of balls, resulting in the mutual convergence and separation of the bearing rings, as well as their roll and slide relative to the raceway grooves [23]. These motions affect the contacts between balls and raceway grooves, affecting the formation of a lubricant film, which not only influences the tribological conditions, but also the electrical conductivity of the lubricated gap between the mating surfaces. Therefore, a detailed bearing dynamics model is the essential pre-requisite for any electro-tribo-dynamic analysis. Sunnersjö [24] investigated the effect of applied inertial forces using an analytical two degree-of-freedom (2-DoF) transversal bearing dynamics model. A 2 DOF of freedom radial deep groove ball bearing model with lubricated contacts under various regimes of lubrication was presented by Rahnejat and Gohar [5]. This

Abbreviations: AC, Alternating current; DC, Direct current; DOF, Degree of freedom; EDD, Electric discharge damage; EHL, Elastohydrodynamic lubrication; ETD, Electro-tribo-dynamic phenomena; FEA, Finite element analysis.

* Corresponding author.
E-mail address: R.Rahmani@lboro.ac.uk (R. Rahmani).

https://doi.org/10.1016/j.triboint.2023.108817
Received 1 June 2023; Received in revised form 3 July 2023; Accepted 19 July 2023
Available online 21 July 2023

Nomenclature

Roman symbols

A_{Hz}	Hertzian contact area m^2.
a_i	Semi-major half-width of an elliptical contact footprint m.
b_i	Semi-minor half-width of an elliptical contact footprint m.
d_b	Ball diameter m.
c	Clearance m.
C	Capacitance F.
D_P	Pitch circle diameter of bearing m.
d_b	Ball diameter m.
e	Curvature sum m.
e_p^*	Footprint ellipticity ratio -
$E_{1,2}$	Young's modulus of elasticity of contacting pair Pa.
$E^{'}$	Effective Young's modulus of elasticity of the contact Pa.
f_b	Base natural frequency of the bearing Hz.
f_c	Cage frequency Hz.
f_{sh}	Shaft rotational frequency Hz.
f_s	Electrical supply frequency Hz.
F_x	Bearing reaction in vertical transverse x-direction N.
F_y	Bearing reaction in lateral transverse y-direction N.
G^*	Dimensionless materials' parameter -
g	Gravitational acceleration m/s^2.
h_i	Lubricant film thickness for the ith contact m.
H_c^*	Dimensionless central film thickness -
i	Electric current A.
K	Contact stiffness non-linearity $N/m^{1.5}$.
K_i	Contact stiffness non-linearity for ball-to-inner race $N/m^{1.5}$.
K_o	Contact stiffness non-linearity for ball-to-outer race $N/m^{1.5}$.
M	Mass of rotor kg.
n	Contact load-deflection exponent -
p_0	Maximum Hertzian contact pressure N/m^2.
p_m	Mean Hertzian contact pressure N/m^2.
Q	Electric charge C.
R	Electrical resistance Ω.
R_{zx}	Effective radius of curvature of the contacting bodies m.
t	Time s.
U	Lubricant entrainment velocity m/s.
U^*	Dimensionless speed (rolling viscosity) parameter -
$V_{ir-b,or-b}$	Voltage across inner or outer race and a ball V.
W_i	Load on the i^{th} rolling element N.
W^*	Dimensionless load parameter -
x,y	Cartesian coordinates m.
$\ddot{x},\ddot{y}$	Lateral radial accelerations m/s^2.
Z	Impedance Ω.
Z_0	Lubricant piezo-viscosity index -
Z_b	Number of balls in the bearing -

Greek Symbols

α_p	Pressure-viscosity coefficient Pa^{-1}.
α,β,λ	Contact dimensional parameters -
δ_i	Contact deflection m.
η_0	Lubricant atmospheric dynamic viscosity Pa.s.
η_e	Lubrincat effective viscosity in the contact Pa.s.
κ_C	Elastic proportionality constant of the contact N/m^2.
ρ	Resistivity Ω.m.
ϕ	Contact angle parameter rad.
ε_0	Magnetic permittivity of free space d.
ε_L	Magnetic permittivity of lubricant d.
θ_i	Peripheral position of the i^{th} ball rad.
$\nu_{1,2}$	Poisson's ratios of contacting pair -

was later extended by Aini et al [25] to a 5 DOF bearing dynamics model. Mohammadpour et al [26] extended the analysis of Rahnejat and Gohar [5] to include the effect of high shear, generated contact heat and lubricant non-Newtonian traction. Faults, cracks, and pits on rolling surfaces, causing secondary bearing vibrations, have also been studied extensively through vibration signal processing of bearings as well as through numerical analysis [27–33].

An experimental investigation was conducted by Joshi and Blennow [34] on ball bearings, exposed to an electric current. The study included the effect of static breakdown voltage upon the lubricant films in ball bearings. It showed that the incidence and duration of the current discharge event was dependent on the voltage, load, and shaft speed. The study was important in showcasing the interactions between the electrical parameters and the dynamic characteristics of rolling element bearings. Becker and Abanteriba [16] presented recent examples of electric discharge damage (EDD) in aviation bearings. The importance of including EDD in the lifespan prediction of aviation rolling element bearings was highlighted. In addition, various damage mechanisms in the form of surface spalls, unusual microcrater damages with and without a heat affected edge, as well as fluting and frosting were noted in [16]. The EDD damage presented in [16] is similar to the ripple-shaped grooves on the outer ring of bearings in wind turbines caused by the displacement of materials from the contacting surfaces as well as some localised melting [17]. Tischmacher and Gattermann [18] investigated bearing damage of variable speed converter-fed electric motors, observing fluting on the surfaces of both the inner and outer races [19]. Fluting, frosting and white etch cracks are common electrically-induced damage patterns [20]. Further examples of electrical fluting on the surface roughness of a ball bearing race are demonstrated in [21]. The study investigated alternating current (AC) motor-shaft voltages and proposed an electrostatic shielded induction motor as a solution to decouple the stator and rotor using a Faraday cage. Other examples of applications include electrical discharge-induced bearing failure in geomagnetic storms in spacecrafts, as well as build-up of charge between the rolling elements and raceways due to lubricant flow in turbines [12].

Prashad [35] evaluated the impedance of rolling element bearings, noting that bearing capacitance reduces with speed, but increases with load at a constant speed. Pashad [36] noted that deterioration of lubricant is an important cause in bearing failure. It has also been shown that an electric current can accelerate lubricant degradation [37]. Magdun and Binder [38] presented Hertzian contact mechanics to determine the capacitance of roller and ball bearings and compared their results with prediction of capacitance from finite element analysis (FEA). It was shown that for ball bearings the capacitance can be determined using the Herzian contact area, whilst for roller bearings an additional area to the Hertzian footprint should be considered. In a combined numerical and experimental investigation Gemeinder [39] presented an impedance model for ball bearings. The investigation highlighted the importance of a full mechanical dynamics model of a bearing. Schneider et al [13] detailed a procedure to determine the capacitance and resistance of an elastohydrodynamic contact and its application to a variety of mechanical sub-systems, including gears and bearings. Schneider et al [40] outlined the importance of bearing capacitance in the prediction of bearing currents. Capacitance distribution in an elastohydrodynamic contact were presented along with a comparison of numerical procedures with the measured data. It was found that the numerical capacitance procedure provided good

agreement with those measured. Schneider et al [41] presented an analytical capacitance method that can monitor the individual film thicknesses of a rolling element complement within a ball bearing. The method used the total capacitance of the ball bearing in order to determine the individual rolling element capacitances. This was achieved by assuming static equilibrium of bearing forces and determining the load distribution within the ball bearing. From this load distribution the distribution of capacitance around the bearing periphery was inferred. The deep groove ball bearing model described in this paper determines the share of dynamic load carried by the ball complement during operation.

This paper presents a 2-DOF bearing tribo-dynamics model with elastohydrodynamics of balls-races contacts. The model is utilised to prescribe the fundamental electrical parameters and study the electrically induced contact phenomena. The highlighted methodology allows individual ball-to-raceway current to be determined, which is difficult to ascertain in practice for the entire rolling element complement through introduction of, for example, ceramic rollers. Therefore, the presented model is viewed as a critical resource for the prediction of bearing performance in combined electro-tribo-dynamic (ETD) conditions. Hitherto, such an integrated multi-physics analysis has not been reported in the literature.

2. Problem Formulation

2.1. Description of Bearing model

The 2-DOF deep groove ball bearing dynamic model is shown in Fig. 1. Lateral motions of the bearing centre determine the share of dynamic load carried by the ball complement during their orbital motion.

To arrive at the 2-DoF bearing dynamics model, the following assumptions are made:

1. The outer and inner bearing rings are perfectly circular.
2. All balls are perfectly spherical with no off-sized balls present.
3. Balls are massless in comparison to the supported shaft.
4. Balls are retained in a cage and evenly-spaced around the bearing's periphery.
5. There are only radial transverse applied bearing loads (no thrust loads).
6. Thermal effects are neglected.
7. The inner and outer races and the supported rotor are considered as rigid (no elastodynamics).
8. Structural/hysteretic and contact damping effects are neglected.
9. The contacts between the ball and the raceways is assumed to comprise a full elastohydrodynamic film. No asperity pair contact is taken into account.

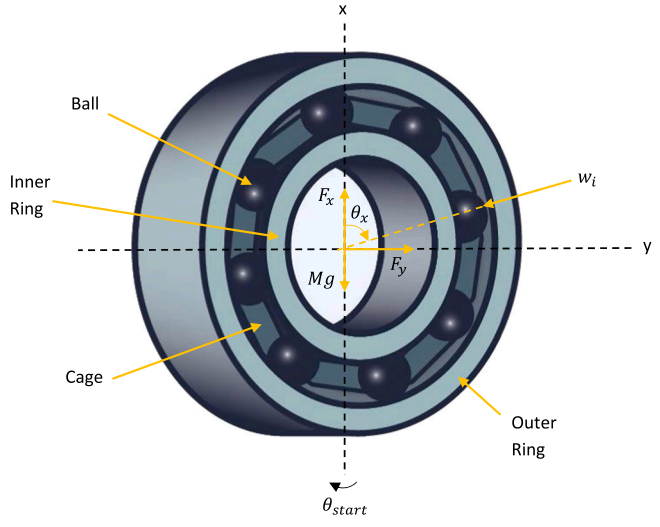

Fig. 1. Schematic representation of a two-degree-of-freedom (2-DoF) deep groove ball bearing model.

The above assumptions lead to a 2-DoF dynamic model described originally in [5,42] for radial deep groove ball bearings. The parametric details of the model have already been described previously in [43,44]. However, for sake of completeness, an outline of the developed tribo-dynamic model is provided here. The model takes into account the x and y radial lateral vibrations of a rigidly mounted shaft (Fig. 1):

The dynamics equations of motion of the bearing centre become:

$$M\ddot{x} = \sum_{i=1}^{m}(-W_i\cos\theta_i) - Mg + F_x \tag{1}$$

$$M\ddot{y} = \sum_{i=1}^{m}(-W_i\sin\theta_i) + F_y \tag{2}$$

where, F_x and F_y are the forces applied externally in the x and y-directions, M is the mass of the supported shaft, θ_i is the angular location of the i^{th} ball and W_i is its corresponding contact reaction, acting radially towards the bearing centre.

Classical Hertzian contact theory describes the balls-to-race contact reactions as:

$$W_i = K\delta_i^n \tag{3}$$

where, δ_i is the localised Hertzian contact deflection of the i^{th} ball, the exponent n is 1.5 for a ball bearing and 1.11 for a roller bearing [1,42,45] and K is the contact stiffness non-linearity. The localised Hertzian contact deflection, δ_i, is given as [42]:

$$2\delta_i = 2(h_i - c) + x\cos\theta_i + y\sin\theta_i \tag{4}$$

where, x and y are the excursions of the bearing centre, c is the radial clearance and h_i is the lubricant film thickness of the i^{th} ball-race contact conjunction.

The combined contact stiffness non-linearity of a ball-inner race and ball-outer race is determined as [46,47]:

$$K = \sqrt{\frac{e}{\lambda^3}}\kappa_C \tag{5}$$

where, e is the combined curvature sum of the ball-to-inner and ball-to-outer raceways as:

$$e = \frac{4}{{R_1}^{-1} + {R_1'}^{-1} + {R_2}^{-1} + {R_2'}^{-1}} \tag{6}$$

where, R_1 is the inner raceway radius of curvature, R_2 is the outer raceway's radius of curvature and R_1' and R_2' are the ball's radii of curvature in the zx and zy contacting planes where for a ball $R_1' = R_2'$. κ_C describes the elastic contact proportionality constant [46]:

$$\kappa_C = \frac{8}{3}\frac{E_1E_2}{E_1(1-\nu_2^2) + E_2(1-\nu_1^2)} \tag{7}$$

λ in Eq. (5) is the ellipticity ratio for the elliptical point contact footprint. α and β are functions of ψ given by [47]:

$$\psi = \cos^{-1}\left[-\frac{e}{4}\sqrt{\left(\frac{1}{R_1}-\frac{1}{R_1'}\right)^2 + \left(\frac{1}{R_2}-\frac{1}{R_2'}\right)^2 + 2\left(\frac{1}{R_1}-\frac{1}{R_1'}\right)\left(\frac{1}{R_2}-\frac{1}{R_2'}\right)\cos 2\phi}\right] \tag{8}$$

where, ϕ is the contact angle parameter, and the corresponding contact parameters are provided in Table 1.

The elliptical contact footprint semi-major and semi-minor half-

Table 1
Contact mechanics parameters [47].

ψ	0^0	10^0	20^0	30^0	35^0	40^0	45^0	50^0	55^0	60^0	65^0	70^0	75^0	80^0	85^0	90^0
α	∞	6.612	3.778	2.731	2.397	2.136	1.926	1.754	1.611	1.486	1.387	1.284	1.202	1.128	1.061	1.00
β	0	0.319	0.408	0.493	0.530	0.567	0.604	0.641	0.678	0.717	0.759	0.802	0.846	0.893	0.944	1.00
λ	-	0.851	1.220	1.453	1.550	1.637	1.709	1.772	1.828	1.875	1.912	1.944	1.967	1.985	1.996	2.00

widths for the i^{th} ball-raceway contact footprint are [46,47]:

$$a_i = \alpha\left(\frac{w_i e}{\kappa_C}\right)^{\frac{1}{3}}, b_i = \beta\left(\frac{w_i e}{\kappa_C}\right)^{\frac{1}{3}} \tag{9}$$

where, the effective contact stiffness for the ball-to-the inner and ball-to-the outer raceways is:

$$K = \left(K_i^{-1/n} + K_o^{-1/n}\right)^{-n} \tag{10}$$

in which, $n = 1.5$. At high contact pressures the pressure distribution in the elastohydrodynamic lubricated (EHL) contact closely follows the dry Hertzian contact pressures. Therefore, the Hertzian pressure distribution in the contact for the individual ball to races contacts is determined as [45]:

$$p(x', y') = p_0\left(1 - \frac{x'^2}{a_i^2} - \frac{y'^2}{b_i^2}\right)^{\frac{1}{2}} \tag{11}$$

where, x' and y' represent the coordinate positions within the ball-races contact footprint and, p_0 is the maximum Hertzian contact pressure given as [45]:

$$p_0 = \frac{3w_i}{2\pi a_i b_i} \tag{12}$$

Assuming isothermal conditions, the instantaneous central contact lubricant film thickness, can be determined for any ball-to-race contact using the Hamrock and Dowson [48] extrapolated lubricant film thickness equation as:

$$H_{ci}^* = 2.69U^{*0.67}G^{*0.53}W^{*-0.067}\left(1 - e^{-0.73\lambda}\right) \tag{13}$$

where, $H_{ci}^* = h_i/R_{zx}$ is the dimensionless central contact lubricant film thickness in which, h_i is the film thickness of the i^{th} ball and R_{zx} is the effective radius of curvature of the contacting bodies acting in the direction of lubricant entrainment (x- direction in the zx plane of contact). The other important dimensionless operating parameters are the speed or rolling viscosity parameter, U^*, the load parameter, W^*, and the material parameter, G^*, given as:

$$U^* = \frac{\eta_0 U}{E' R_{zx}}, W_i^* = \frac{w_i}{E' R_{zx}^2}, G^* = E'\alpha_p, \lambda = \frac{a_i}{b_i} \tag{14}$$

where, U is the speed of lubricant entrainment into the contact, η_0 is the atmospheric dynamic viscosity of the lubricant, α_p is the lubricant piezo-viscosity coefficient and E' is the equivalent (effective) Young's modulus of elasticity of the contacting bodies:

$$E' = 2\left(\frac{1 - \nu_1^2}{E_1} + \frac{1 - \nu_2^2}{E_2}\right)^{-1} \tag{15}$$

The effective viscosity of the lubricant in the contact for the sake of computational convenience can be approximated by the Roelands model as [49]:

$$\eta_e = \eta_0 \exp\left\{\ln\left(\frac{\eta_0}{\eta_\infty}\right)\left[\left(1 + \frac{p_m}{C_p}\right)^{Z_0} - 1\right]\right\} \tag{16}$$

where, $\eta_\infty = 6.31 \times 10^{-5} Ns/$, $C_p = 1.96 \times 10^8 Pa$, are Roelands' constants and the lubricant piezo-viscosity index is: $Z_0 = C_p\alpha_p / \ln\left(\frac{\eta_0}{\eta_\infty}\right)$.

The bearing specifications are listed in Table 2. A 5 μm radial interference fit is applied to mitigate undesired phenomena such as emergence of clearance in contact zones leading to ball skidding, rattling and cage collisions. Therefore, all the ball-to-raceway contacts remain in compression throughout their orbital cycle, justifying the use of the classical Hertzian contact theory. The radii of curvature of the raceways' grooves provides a contact conformity of 7% as well as a contact angle parameter of $\phi = 45^0$.

Table 2
Bearing specifications [43,44].

Parameter	Value	Unit
Bore	40	mm
Inner race diameter	50	mm
Pitch diameter	56.3	mm
Outer race inner diameter	75.4	mm
Outer race outside diameter	83.7	mm
Width	23.4	mm
Number of rollers	12	-
Ball diameter	12.7	mm
Effective contact stiffness	13.509	$GN/m^{1.5}$
α, β	1.5, 0.5	–
Ellipticity ratio	2.5	–
Young modulus	210	GPa
Poisson ratio	0.3	–
Lubricant dynamic viscosity (at 60 °C)	0.08	Pa.s
Piezo-viscosity coefficient (at 60 °C)	1.44×10^{-8}	Pa^{-1}
Lubricant relative permittivity	2.65	–
Lubricant resistivity	1×10^{10}	Ω.m

2.2. Contact electric circuit model

The electric circuit diagram for an individual rolling element is shown in Fig. 2. The applied voltage is dependent on the voltage differential from the inner ring to the outer ring. The electric current passes through the inner bearing ring-ball contact, the ball itself, and then onto the outer ring-ball contact.

The following assumptions are made in the electrical discharge model:

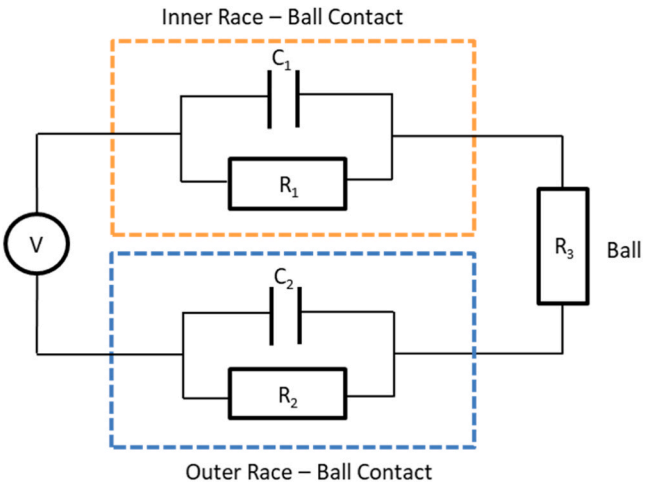

Fig. 2. Electrical contact model.

- The bearing has an insulating cage.
- The resistance of the metallic ball and its capacitance are considered negligible in comparison to those of the lubricant film.

Using Kirchhoff's voltage law, the total voltage drop is due to the existence of the lubricating medium formed between the ball and inner race and ball and outer race contacts. These are considered to be in a series circuit, thus:

$$V_T = V_{ir-b} + V_{or-b} \tag{17}$$

The total impedance of the circuit is given as:

$$Z_T = Z_{ir-b} + Z_{or-b} \tag{18}$$

Therefore, the electric current becomes:

$$i_T = \frac{V_T}{Z_T} = \frac{V_{ir-b} + V_{or-b}}{Z_{ir-b} + Z_{or-b}} \tag{19}$$

In addition, the electric charge stored in a capacitor is determined as:

$$Q = CV \tag{20}$$

The electric current is the rate of change of charge, thus:

$$i = \frac{dQ}{dt} \tag{21}$$

Using the Leibniz product rule and replacing for Q from Eq. (20), one obtains:

$$i = \frac{dQ}{dt} = C\frac{dV}{dt} + V\frac{dC}{dt} \tag{22}$$

where, $C\frac{dV}{dt}$ includes the electrical capacitance and the instantaneous rate of change of voltage, while $V\frac{dC}{dt}$ incorporates the voltage and the rate of change of capacitance with time. The latter is often not utilised in the electrical engineering field applications, whilst it can have an important effect in tribological applications as outlined in the current study. However, in tribological applications such as in the study of rolling element bearings, subjected to an electrical current, the latter term in Eq. (22) is ignored due to the usual assumption of steady-state conditions. In real applications, the capacitance effect due to the dielectric properties of the lubricant is subjected to variation as the film thickness varies during the bearing operation. Under conditions of variable load, the Hertzian contact area can also alter in time. Such changes in the capacitance with time, if subjected to high voltages, can produce a comparable term in magnitude to the first term on the right-hand side of Eq. (22). Therefore, it should be considered in such cases.

For tribological contacts the capacitance is calculated using [39,40]:

$$C = k_c \varepsilon_0 \varepsilon_L \frac{A_{Hz}}{h_c} \tag{23}$$

where, A_{hz} is the Hertzian contact area given as:

$$A_{Hz} = \pi ab \tag{24}$$

a and b are the Hertzian contact footprint semi-half-widths and h_c is the central lubricant film thickness for a contact subject to EHL obtained from Eq. (14). ε_0 is the vacuum permittivity, ε_L is the relative permittivity of the lubricant and k_c is the ratio of the total capacitance to the capacitance of the Hertzian contact [39,40].

The current passing through a resistor is given as:

$$i = \frac{V}{R} \tag{25}$$

where, R is the electrical resistance and in the case of an EHL contact is [39]:

$$R = \frac{\rho h_c}{A_{Hz}} \tag{26}$$

in which, ρ is the resistivity of the lubricant.

Thus, for a single inner race-ball-outer race contact the current is determined by super-positioning of Eqs. (22) and (26) as:

$$i = C\frac{dV}{dt} + \left(\frac{dC}{dt} + \frac{1}{R}\right)V \tag{27}$$

The presence of an electrical potential difference between the inner and outer rings of the ball bearing allows for the passage of an electric current across the inner-ball-outer race contact. Therefore, expanding Eq. (27) for a complement of balls in their orbital path, one obtains:

$$\begin{bmatrix} i_1 \\ \vdots \\ i_n \end{bmatrix} = \frac{dV}{dt}\begin{bmatrix} C_1 & \cdots & 0 \\ \vdots & \ddots & \vdots \\ 0 & \cdots & C_n \end{bmatrix} + V\begin{bmatrix} \frac{dC_1}{dt} + \frac{1}{R_1} & \cdots & 0 \\ \vdots & \ddots & \vdots \\ 0 & \cdots & \frac{dC_n}{dt} + \frac{1}{R_n} \end{bmatrix} \tag{28}$$

The individual electric power passed through each contact can be determined accordingly, using:

$$P_n = i_n V \tag{29}$$

3. Method of solution

A multi-physics 2-DOF rolling element bearing electro-tribo-dynamics model that includes the elastohydrodynamics of balls-races contacts as well as an integrated electrical resistance and capacitance model of the lubricant films is developed in the current study. To solve the associated governing equations, a numerical solution approach is developed. Details of the solution procedure is depicted in the flowchart of Fig. 3.

4. Results and discussion

A full description including the validation of the ball bearing model

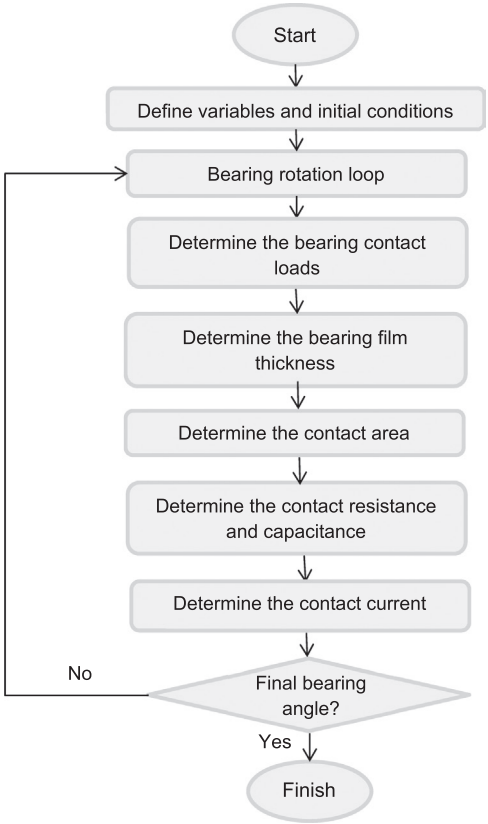

Fig. 3. Numerical solution procedure.

presented in this paper is provided in [43,44]. The bearing undergo rotation at a constant speed, corresponding to a cage frequency of 13.3 Hz. There is a complement of 12 balls, representing a moderately packed arrangement. The radii of curvature of the raceways' grooves ensures a 7% contact conformity and a contact angle parameter of $\phi = 45^0$. A radial interference fit of − 5 μm ensures that there would be no emerging clearances. Therefore, all the balls-to-races contacts remain in compression under the applied load, and the lubricant film thickness remains in EHL. The presence of unloaded zones can lead to excess noise and vibration and is typical of an insufficiently interference fitted or preloaded bearing. Fig. 4(a) shows the ball-race contact reaction for a single cage cycle, whilst Fig. 4(b) demonstrates cyclic ball-to-races contact lubricant film thickness for a single cage cycle. Fig. 4(c) shows the corresponding frequency spectrum of the lubricant film thickness roof ripple oscillations for several cage cycles. The fundamental bearing frequencies appear in the lubricant film ripple oscillations, including $f_b = D_p f_{sh}/(2d_b)$, where D_P is the bearing pitch circle diameter, d_b is the nominal ball diameter and f_{sh} is the shaft frequency. These correspond to the base natural frequency of the system, and is dependent on the bearing load, as well as its dynamic stiffness [5,42].

Cage frequency is the other main frequency of the system due to the variation of film thickness in a typical ball orbital motion. This results in bearing vibrations as a function of the cage rotational speed. This has been shown both analytically and experimentally by Wardle [6] and Lynagh et al [7], as $f_c = 0.5 f_{sh}(1 - d_b \cos\phi / D_P) = 13.3Hz$. In the current investigation this corresponds to the predicted numerical bearing cage frequency of 13.27*Hz* as shown in Fig. 4(c). Modulations of the system natural frequency and the multiples of the cage frequency are also present in the response.

Now an AC voltage supply frequency, f_s, is applied to the model at an amplitude of 60 V and frequency of 20 Hz. The current across the fluid film for five orbital cycles is shown in Fig. 5(a). An important modulation $f_m = f_s - f_c$ links the mechanical and electrical frequency components (mechanical spectral contributions in Fig. 4(b) with those of electrical nature in Fig. 5(b)). This modulation contains a component linked to the voltage supply frequency, f_s, and the cage frequency, f_c. Critically, this is also linked to the bearing base natural frequency, f_b. This links a host of mechanical bearing parameters such as rotational speed, bearing load, dynamic stiffness, interference, preload, and number of balls in the bearing to the electrical current parameters. The load and speed dependence of the breakdowns have been experimentally observed in [34,35]. The bearing base frequency and its modulations are of significantly greater magnitude in the current breakdowns of Fig. 5(b) than in the vibration response of Fig. 4(b). This demonstrates the influence of the change in capacitance term (dC/dt) driven by oscillations in film thickness and the contact area variations on the predicted electrical current by Eq. (27). The high frequency components of vibration have a larger influence as they cause rapid fluctuations in electrical capacitance, and thus the induced current. Electrical loading can cause damage to raceways and balls through electrical discharge erosion [17,21,50]. With a high electric current, the discharge causes localised high temperature regions on the surface and can result in the formation of surface pits [51]. In low current breakdowns frosting typically occurs which can result in pitting damage over time, as well as carbonisation and oxidation of the lubricant [51]. The electric current profile in Fig. 5(a) contains high amplitude discharges as well as low amplitude oscillations, demonstrating the possibility for both types of wear. The electric current oscillations, predicted around the orbital

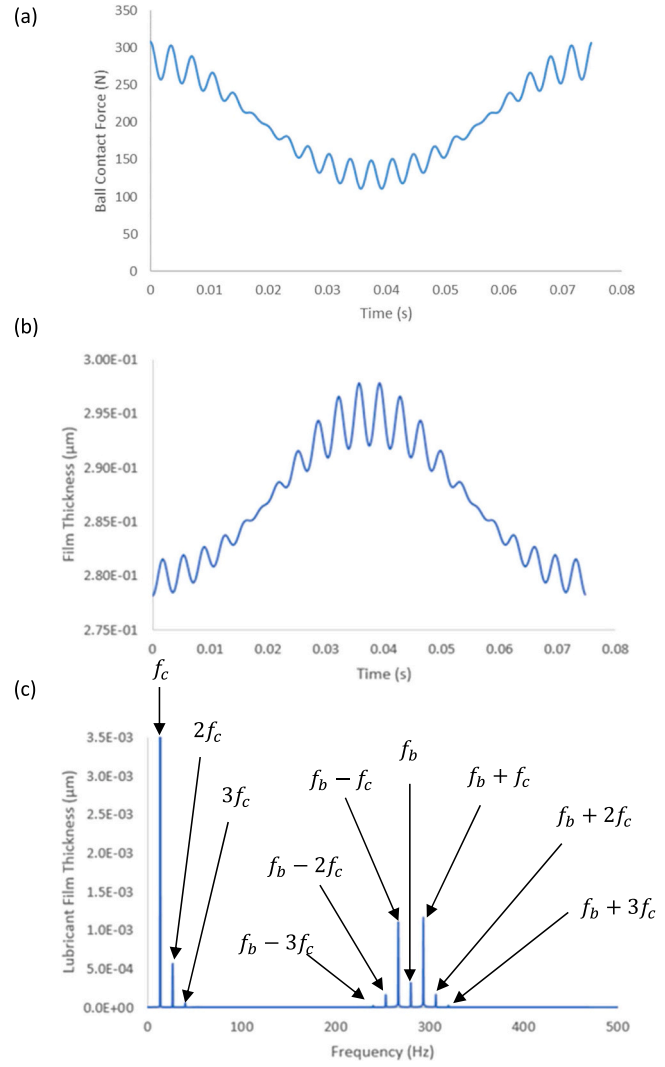

Fig. 4. (a) Ball contact force (b) Lubricant film thickness per ball-to-races contact in a cage cycle, and (c) frequency spectrum of lubricant film thickness.

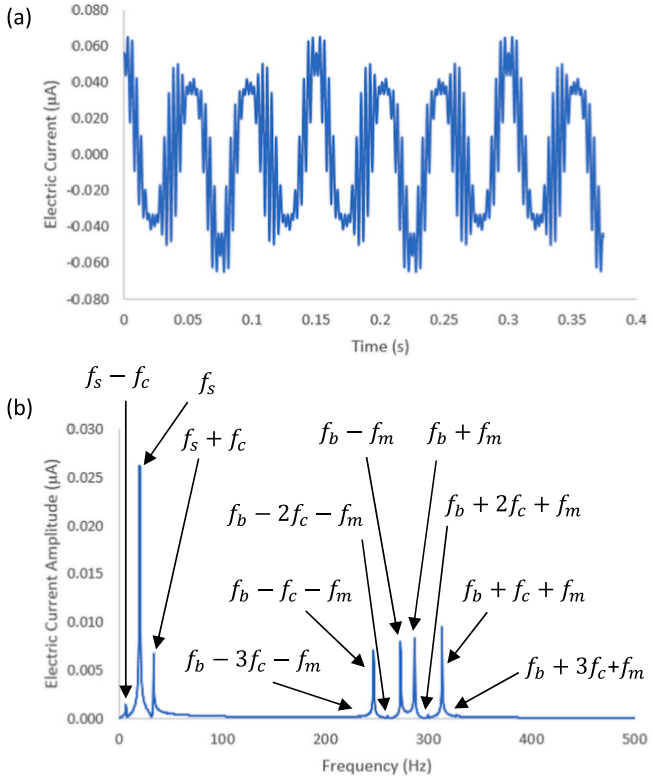

Fig. 5. (a) Electric current profile across a ball-to-races contact in five cage cycles, (b) frequency spectrum of the electric current profile.

cycle, correlates with the periodic ripple-shaped grooves observed in electrical erosion failures [16–22]. The applied voltage causes a breakdown current across the bearing, resulting in surface damage in the form of frosting, fluting and spalling, as well as oxidation of the lubricant [14]. Komatsuzaki et al [37] showed that electric current can accelerate lubricant degradation, and its importance in bearing failure [36]. Ripple-shaped grooves are a common electrically induced damage pattern, often observed in aviation propulsion bearings [16], bearings in wind turbines [17], and those of the electric motors [18,19,21]. Variations in lubricant film thickness around the bearing periphery cause changes in the electric current, which when initiated, would lead to other bearing damage mechanisms to occur [14]. This highlights the importance of combined electro-tribo-dynamics modelling for prediction of electrical contact phenomena in ball bearings.

Fig. 6(a) shows the instantaneous electrical power across the film. The instantaneous power is an important indicator in determining the quantity of energy transferred into the surfaces which can potentially cause electrical discharge damage. Fig. 6(b) displays the frequency spectrum of the power profile. The major frequency components such as cage frequency, base natural frequency and supply voltage frequency are all present as identified in Fig. 6(b).

The supply voltage, f_s diminishes in response to the power discharge through the contact. This is because the power is driven fundamentally by a change in capacitance as well as any change in the voltage. Combining Eqs. (27) and (29) for power, yields:

$$P = VC\frac{dV}{dt} + \left(\frac{dC}{dt} + \frac{1}{R}\right)V^2 \tag{30}$$

Eq. (30) represents the component $2f_s$ in Fig. 6(b). The discharged current of the capacitor reaches its maximum value when the rate of change in voltage is the greatest. However, the electric power is highest when the absolute voltage attains its greatest value. This results in the two peaks per a voltage cycle, f_s. Therefore, from Fig. 6(b) it can be seen that the contributions due to capacitance (the first term on the right-hand side of Eq. (22)) are low in the power discharge due to the absence of high magnitude frequency components, containing the voltage power source fundamental frequency. There are modulations of the voltage supply frequency, f_s, with the base natural frequency of the system, f_b linking the supply frequency, f_s with a number of mechanical parameters of the system. The power contributions due to resistance and a change in capacitance are greater than that observed in the breakdown of the current. This is because they are dependent on the magnitude of the square of the voltage. This is evident in the frequency response, as the modulations with respect to mechanical frequencies such as cage frequency and the system base natural frequency are substantially higher in amplitude. The importance of ensuring that the first harmonic of the voltage supply frequency $(2f_s)$ cage frequency (f_c) and the base frequency (f_b) do not coincide is evident in this detailed analysis. The electrical power within the contact is a means for the sudden discharge of stored electrical potential energy which can cause electrical energy damage to the bearing components.

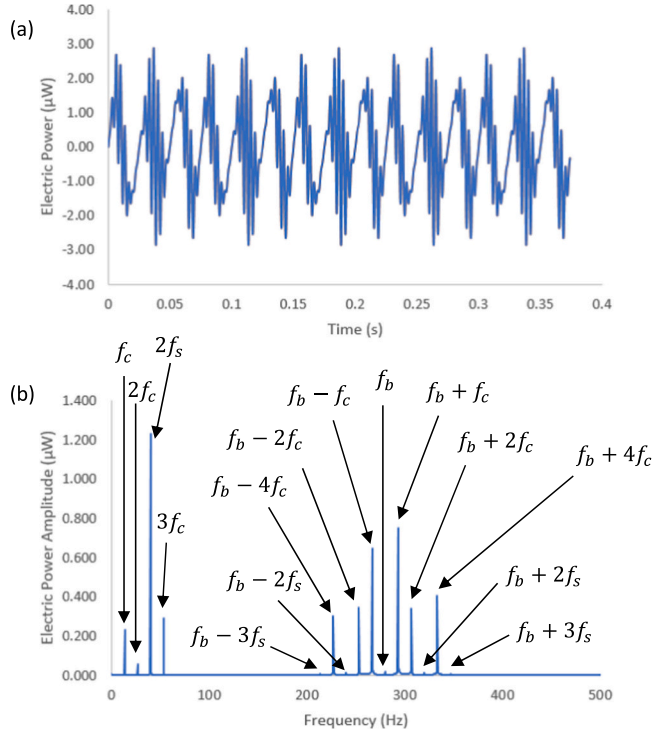

Fig. 6. (a) Power discharge across a ball-to-races contact in five cage cycles, (b) frequency spectrum of the power discharge profile.

Fig. 7 shows the electrical power density stored within the lubricant film. The power density includes the positive and negative parts of the voltage cycle. It describes the mechanism of the transfer of the current from the inner ring to the outer ring as the power source provides an alternating voltage differential across the bearing. The total power demonstrates the energy that can be dissipated across the lubricant film and cause localised high temperature regions on surfaces which can lead to pitting [50].

In practice, it is possible for a system to be subjected to an AC supply voltage, as well as a DC supply voltage. The AC voltage supply frequency, f_s is incrementally linearly swept from 0 Hz to 100 Hz over 25 cage cycles. As the AC voltage supply frequency diminishes, the system increasingly behaves similar to that subjected to a DC voltage alone. The power contributions due to resistance and any change in capacitance, representing the second term in Eq. (30) are presented in Fig. 8(a). The contributions due to the change in voltage (first term in Eq. (30)) are presented in Fig. 8(b). Both responses are dominated by rhythmic fluting, prescribed by the bearing cage cycle, which is in addition to the various system fundamental frequencies such as the bearing base natural frequency and the electrical supply frequency and their modulations. This demonstrates the importance of cage frequency in subsequent breakdowns. The bearing base natural frequency dominates the breakdown at low voltage supply frequencies, including for a DC voltage. Fundamentally, at low voltage supply frequencies, the contributions of $4f_s$ are quite low due to a small rate of change of voltage, and the two modulations $f_b + 4f_s$ and $f_b - 4f_s$ tend to converge. As the supply frequency increases the two modulations $f_b + 4f_s$ and $f_b - 4f_s$ diverge and the contribution at $4f_s$ plays a dominant role in combination with the cage frequency. These frequencies propagate through the system in bands of $4f_s$, $f_b + 4f_s$ and $f_b - 4f_s$. An important mechanical resonance condition arises when the base natural frequency (f_b) coincides with $4f_s - f_b$ or $f_s \approx 0.25f_b$. This frequency is critical for the evaluation of a bearing optimal design when considering applications with electrical current

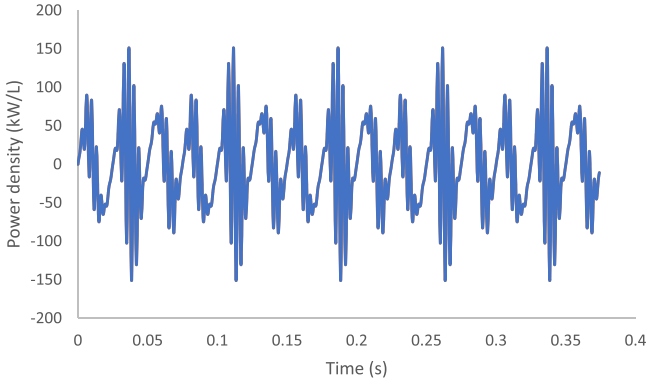

Fig. 7. Indicative electric power density stored in the lubrication fluid film across 5 cage cycles.

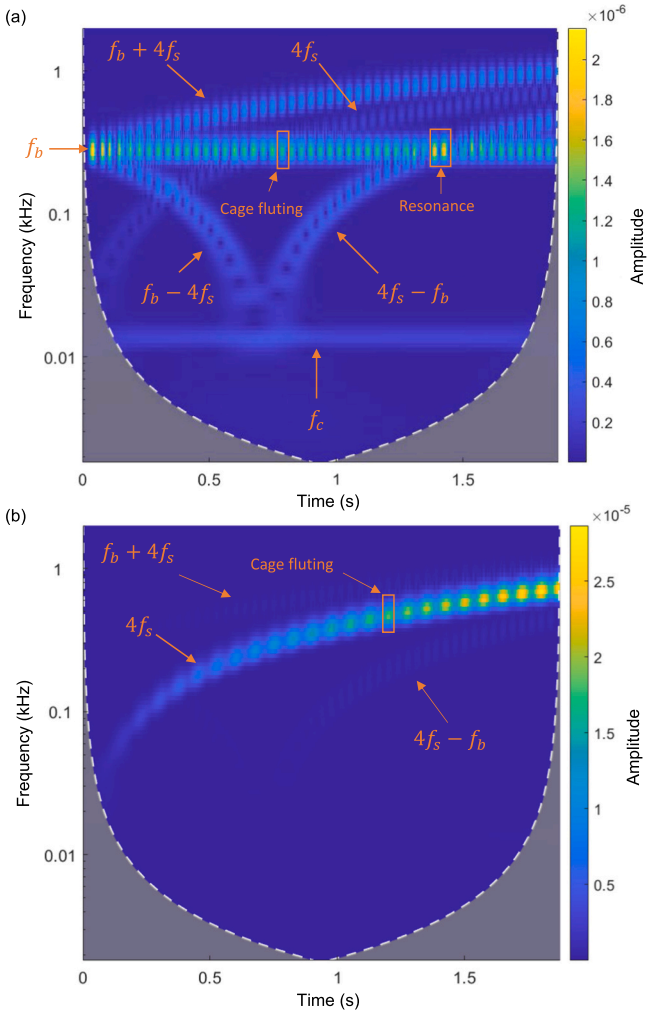

Fig. 8. Predicted results showing the effect of a 0–100 Hz voltage frequency sweep on the power discharge across the ball-to-races contact: (a) contributions due to resistance and change in capacitance, (b) contributions due to capacitance.

exposure. It is important to consider that alongside this issue, there is a substantial envelope for overlap through modulations as identified in Fig. 6(b) such as $f_b + f_c$. The rhythmic fluting occurs at f_c in Fig. 8(b), and $2f_c$ in Fig. 8(a) due to the influence of the rate of change of capacitance in Fig. 8(a), and the direct relationship with capacitance in Fig. 8 (b). The predicted rhythmic electric power across the ball-to-races contacts in their orbital motion during a voltage frequency sweep correlates with the periodic ripple-shaped grooves observed in electrical erosion failures. Variations in the lubricant film thickness around the bearing periphery cause corresponding changes in the generated electric current which induce normal modes of bearing damage [14]. Fig. 8 highlights the importance of the fundamental mechanical-based dynamic frequencies and their influence upon the lubricant film thickness of various contacts around the bearing periphery. The rhythmic pulsing around the bearing periphery correlates with the ripple-shaped groove damage pattern often observed in practice and reported in the open literature [16–19, 21]. This demonstrates the importance of including a combined electro-tribo-dynamic model in the analysis of such systems. The rhythmic cage fluting observed in Fig. 8(b) ensures that even when there is a high frequency voltage, the response is determined by the magnitude of capacitance and resistance. These are affected by tribological operational parameters such as lubricant film thickness and contact area. High frequency voltages are a by-product of electrical machines fed by frequency inverters that approximate a sinusoidal voltage with a series of pulses. In such applications the voltage frequency is typically much greater than 100 Hz. This is referred to as a common mode voltage that can result in high frequency bearing currents and electrical discharge damage [13].

5. Concluding remarks

An integrated multi-physics model of radial deep groove ball bearing comprising dynamics, contact mechanics/tribology and an electrical contact circuit model is developed. The model includes the effect of electrical capacitance and resistance in rolling contacts. The electrical capacitance model includes the changes in voltage and variations in the capacitance itself. Bearing dynamics influence the lubricant film thickness and contact area of balls-inner race and balls-outer race contacts. In turn, these would affect the electrical contact capacitance and resistance.

The results show that the electric current passing through the bearing is fundamentally linked to its base natural frequency and the cage rotational frequency. It is already known that the electric current can cause damage to the raceways and the balls' complement through electrical discharge erosion. The results from the developed model show that the potential damage caused by the electric current can be directly attributed to a host of mechanical and operational bearing parameters such as rotational speed, bearing load, dynamic stiffness, interference fit and number of balls in the rolling element complement. The importance of these parameters on electrical damage in a host of systems, including the effect of lubricant degradation on their performance is highlighted.

An important modulation effect between the voltage supply frequency and the bearing cage frequency is observed in the passage of the electric current through the rolling contacts, associated with the harmonics of the cage frequency, as well as the bearing base natural frequency. The effect of the supply frequency and the magnitude of voltage in the total contact electrical power is shown along with the coincidence of fundamental frequencies and their modulations, such as that between the voltage supply frequency (f_s) and the cage frequency (f_c) as well as the base natural frequency (f_b). The total contact electrical power increases with any rise in the electrical supply frequency as it is directly proportional to it. The influence of cage frequency on the rhythmic fluting, observed in the electrical power across the ball-to-races contact, is also demonstrated. A frequency sweep from DC voltage to AC voltage shows the dominance of the bearing base natural frequency (f_b) and the cage frequency (f_c).

The main original contribution of the current study is the demonstration of a direct link between the electrical fluting and the bearing vibration spectral content. Furthermore, the model presented in this study allows the investigation of electric current discharge for a single contact in isolation, which is critical for the validation of bearing performance. Consideration of the effect of operating under mixed regime of lubrication can provide an interesting addition to the current work.

Declaration of Competing Interest

Hereby, it is confirmed that there are no competing interests to be declared.

Data Availability

Data will be made available on request.

Acknowledgement

The authors gratefully acknowledge the financial support of Engineering and Physical Sciences Research Council (EPSRC) under the Centre for Doctoral Training in Embedded Intelligence (CDT-ei); grant reference EP/L014998/1.

Statement of Originality

Hereby, it is confirmed that this manuscript reflects on original research conducted solely by the authors of this manuscript. This manuscript has not been published, nor is under consideration for publication elsewhere.

References

[1] Harris, T.A., Rolling bearing analysis, John Wiley and Sons, 2001.
[2] Johns-Rahnejat, P.M. and Gohar, R., Point contact elastohydrodynamic pressure distribution and sub-surface stress field, In International Tri-Annual Conference on Multi-Body Dynamics: Monitoring and Simulation Techniques, Bradford, UK, 1997, pp. 161–177.
[3] Rubini R, Meneghetti U. Application of the envelope and wavelet transform analyses for the diagnosis of incipient faults in ball bearings. Mech Syst Signal Process 2001;15(2):287–302.
[4] Yhland E. A linear theory of vibrations caused by ball bearings with form errors operating at moderate speed. J Tribology 1992;114(2):348–59.
[5] Rahnejat H, Gohar R. The vibrations of radial ball bearings. Proc IMechE, Part C: J Mech Eng Sci 1985;199(3):181–93.
[6] Wardle FP. Vibration forces produced by waviness of the rolling surfaces of thrust loaded ball bearings Part 1: theory. Proc IMechE, Part C: J Mech Eng Sci 1988;202 (5):305–12.
[7] Lynagh N, Rahnejat H, Ebrahimi M, Aini R. Bearing induced vibration in precision high speed routing spindles. Int J Mach Tools Manuf 2000;40(4):561–77.
[8] Kim SM, Lee SK. Prediction of thermo-elastic behavior in a spindle–bearing system considering bearing surroundings. Int J Mach Tools Manuf 2001;41(6):809–31.
[9] Grujičić RN, Tomović RN, Mitrović RM, Jovanović JD, Atanasovska ID. The analysis of impact of intensity of contact load and angular shaft speed on the heat generation within radial ball bearing. Therm Sci 2016;20(5). 133-133.
[10] He F, Xie G, Luo J. Electrical bearing failures in electric vehicles. Friction 2020;8 (1):4–28.
[11] Zhang P, Neti P, Salem S. Electrical discharge and its impact on drivetrains of wind turbines. IEEE Trans Ind Appl 2015;51(6):5352–7.
[12] Bialke W. A discussion of friction anomaly signatures in response to electrical discharge in ball bearings. Aerosp Mech Symp 2018;44:55–68.
[13] Schneider V, Behrendt C, Höltje P, Cornel D, Becker-Dombrowsky FM, Puchtler S, et al. Electrical bearing damage, a problem in the nano-and macro-range. Lubricants 2022;10(8):194.
[14] Kowal, D., Bearing damage resulting from shaft voltages and currents, Application Note, Computational Systems Inc., USA, 1999.
[15] Costello MJ. Shaft voltages and rotating machinery. IEEE Tran Ind Appl 1993;29 (2):419–26.
[16] Becker A, Abanteriba S. Electric discharge damage in aircraft propulsion bearings. Proc IMechE, Part J: J Eng Tribology 2014;228(1):104–13.
[17] Peng H, Zhang H, Fan Y, Shangguan L, Yang Y. A review of research on wind turbine bearings' failure analysis and fault diagnosis. Lubricants 2023;11(1):14.
[18] Tischmacher H, Gattermann S. Multiple signature analysis for the detection of bearing currents and the assessment of the resulting bearing wear. Int. Sympos. Power Electronics, Electrical Drives, Automation and Motion. IEEE; 2012. p. 1354–9.
[19] Tischmacher H. Systemanalysen zur elektrischen Belastung von Wälzlagern bei umrichtergespeisten Elektromotoren. Gottfried Wilhelm Leibniz Univ, Hann 2017. X-225.
[20] Gould B, Demas N, Erck R, Lorenzo-Martin MC, Ajayi O, Greco A. The effect of electrical current on premature failures and microstructural degradation in bearing steel. Int J Fatigue 2021;145:106078.
[21] Busse D, Erdman J, Kerkman RJ, Schlegel D, Skibinski G. System electrical parameters and their effects on bearing currents. IEEE Trans Ind Appl 1997;33(2): 577–84.
[22] Joshi, A., Electrical Characterisations of Bearings, PhD Thesis, High Voltage Engineering, Electrical Engineering, Chalmers University, Sweden, 2019.
[23] Kushwaha M, Rahnejat H. Transient concentrated finite line roller-to-race contact under combined entraining, tilting and squeeze film motions. J Phys, D: Appl Phys 2004;37(14):2018.
[24] Sunnersjö CS. Varying compliance vibrations of rolling bearings. J Sound Vib 1978; 58(3):363–73.
[25] Aini R, Rahnejat H, Gohar R. A five degrees of freedom analysis of vibrations in precision spindles. Int J Mach Tools Manuf 1990;30(1):1–18.
[26] Mohammadpour M, Johns-Rahnejat PM, Rahnejat H. Roller bearing dynamics under transient thermal-mixed non-Newtonian elastohydrodynamic regime of lubrication. Proc IMechE, Part K: J Multi-body Dyn 2015;229(4):407–23.
[27] Meyer LD, Ahlgren FF, Weichbrodt B. An analytic model for ball bearing vibrations to predict vibration response to distributed defects. J Mech Des 1980;102(2): 205–10.
[28] Ho D, Randall RB. Optimisation of bearing diagnostic techniques using simulated and actual bearing fault signals. Mech Syst Signal Process 2000;14(5):763–88.
[29] Sopanen J, Mikkola A. Dynamic model of a deep-groove ball bearing including localized and distributed defects. Part 1: theory. Proc IMechE, Part K: J Multi-body Dyn 2003;217(3):201–11.
[30] Patel UA, Naik BS. Nonlinear vibration prediction of cylindrical roller bearing rotor system modeling for localized defect at inner race with finite element approach. Proc IMechE, Part K: J Multi-body Dyn 2017;231(4):647–57.
[31] Smith WA, Randall RB. Rolling element bearing diagnostics using the case western reserve university data: a benchmark study. Mech Syst Signal Process 2015;64: 100–31.
[32] Vafaei S, Rahnejat H, Aini R. Vibration monitoring of high speed spindles using spectral analysis techniques. Int J Mach Tools Manuf 2002;42(11):1223–34.
[33] Ghaisas N, Wassgren CR, Sadeghi F. Cage instabilities in cylindrical roller bearings. J Tribology 2004;126(4):681–9.
[34] Joshi A, Blennow J. Investigation of the static breakdown voltage of the lubricating film in a mechanical ball bearing. Proc Nord Insul Symp 2013:23.
[35] Prashad H. Investigations of corrugated pattern on the surfaces of roller bearings operated under the influence of electrical fields. Lubr Eng 1988;44(8):710–7.
[36] Prashad H. Theoretical evaluation of impedance, capacitance and charge accumulation on roller bearings operated under electrical fields. Wear 1988;125 (3):223–39.
[37] Komatsuzaki S, Uematsu T, Nakano F. Bearing damage by electrical wear and its effect on deterioration of lubricating greases. Lubr Eng 1987;43(1):25–30.
[38] Magdun O, Binder A. Calculation of roller and ball bearing capacitances and prediction of EDM currents. 2009 35th Annu Conf IEEE Ind Electron 2009:1051–6.
[39] Gemeinder Y, Schuster M, Radnai B, Sauer B, Binder A. Calculation and validation of a bearing impedance model for ball bearings and the influence on EDM-currents. 2014 Int Conf Electr Mach (ICEM) 2014:1804–10.
[40] Schneider V, Liu HC, Bader N, Furtmann A, Poll G. Empirical formulae for the influence of real film thickness distribution on the capacitance of an EHL point contact and application to rolling bearings. Tribology Int 2021;154:106714.
[41] Schneider V, Bader N, Liu H, Poll G. Method for in situ film thickness measurement of ball bearings under combined loading using capacitance measurements. Tribology Int 2022;171:107524.
[42] Rahnejat H. Computational modelling of problems in contact dynamics. Eng. Anal. 1985;2(4):192–7.
[43] Turnbull R, Rahmani R, Rahnejat H. The effect of outer ring elastodynamics on vibration and power loss of radial ball bearings. Proc Inst Mech Eng, Part K: J Multi-body Dyn 2020;234(4):707–22.
[44] Turnbull R, Dolatabadi N, Rahmani R, Rahnejat H. Nonlinear tribodynamics of an elastic shaft with a flexible bearing outer race. Proc Inst Mech Eng Part K: J Multi-Body Dyn 2023. https://doi.org/10.1177/14644193231161136.
[45] Gohar, R. and Rahnejat, H., Fundamentals of Tribology, 2nd Edition, World Scientific Publishing Company, 2012.
[46] Hoffmann, F. and Rahnejat, H., Constrained Multi-body Dynamic Analysis of Shaft and Bearing Systems, In Vibration and Control of Mechanical Systems, 2001: Presented at the 2001 ASME International Mechanical Engineering Congress and Exposition, November 11–16, 2001, New York.
[47] Whittemore, H.L. and Petrenko, S.N., Friction and Carrying Capacity of Ball and Roller Bearings, National Bureau of Standards, Technical Paper 201, Washington DC, 1921.
[48] Hamrock BJ, Dowson D. Isothermal elastohydrodynamic lubrication of point contacts: part III—fully flooded results. J Lubr Technol 1977;99(2):264–75.
[49] Roelands, C.J.A., "Correlational aspects of the viscosity-temperature-pressure relationship of lubricating oils", Dissertation, University of Delft, Netherlands, 1966.
[50] Morris SA, Leighton M, Morris NJ. Electrical field strength in rough infinite line contact elastohydrodynamic conjunctions. Lubricants 2022;10(5):87.
[51] ISO 15243:2017, Rolling Bearings—Damage and Failures—Terms, Characteristics and Causes, International Organization for Standardization: Geneva, Switzerland. March 2017.